

Diagrammatic method for the theory of magnetic and resistive properties of manganites

This article has been downloaded from IOPscience. Please scroll down to see the full text article.

2006 J. Phys.: Condens. Matter 18 6699

(<http://iopscience.iop.org/0953-8984/18/29/011>)

View [the table of contents for this issue](#), or go to the [journal homepage](#) for more

Download details:

IP Address: 129.252.86.83

The article was downloaded on 28/05/2010 at 12:22

Please note that [terms and conditions apply](#).

Diagrammatic method for the theory of magnetic and resistive properties of manganites

E E Zubov¹, V P Dyakonov^{1,2} and H Szymczak²

¹ A A Galkin Donetsk Physics and Technology Institute NASU, 83114 Donetsk, Ukraine

² Institute of Physics, PAS, 02-669 Warsaw, Poland

E-mail: zubov@dyakon.fti.ac.donetsk.ua

Received 14 November 2005, in final form 6 June 2006

Published 30 June 2006

Online at stacks.iop.org/JPhysCM/18/6699

Abstract

A diagrammatic method for the theory of magnetic and resistive properties of manganites has been applied. The Holstein double-exchange model for a narrow band with the strong Hund's rule coupling was studied. In parallel with the Lang–Firsov unitary transformation of the zeroth Hamiltonian, we have realized the diagonalization of Hund's Hamiltonian neglecting the upper triplet. The diagram techniques taking into account the quantum spin fluctuations of the lower quintet and hole state with spin $S = 3/2$ were developed. The magnetic structure of the ground state and an influence of electron–phonon interaction have been analysed using the first nonvanishing approximation of the perturbation theory. Since a simple self-consistent equation for the Green function is lacking, the approximations for the effective interaction line with strong electron–phonon coupling were used. The influences of quantum fluctuations and electron–phonon interactions on magnetization, the Curie temperature and resistivity were investigated. The calculated temperature dependence of resistivity in the pure double-exchange model agrees well with experimental data.

1. Introduction

An investigation of the thermodynamics of the double-exchange (DE) model is urgently required because a theory taking into account the quantum nature of electron and ion spins sequentially is still lacking. In manganites with dominant DE and strong electron correlations, strong Hund's rule coupling of the collective e_g electron with the Mn^{4+} ion spin should be considered. This essentially extends the wavefunction basis used and creates some difficulties in the construction of diagram techniques. Anderson and Hasegawa [1] have calculated the spectrum of electron excitation exactly in a system of two multivalent ions Mn^{3+} and Mn^{4+} . De Gennes [2] has studied the thermodynamics of this system for a system of classical spins neglecting strong electron correlations. Kubo and Ohata [3] have proposed an exact projective

transformation of the Hamiltonian with Hund's rule coupling. Unfortunately, because of the complicated dependence of this transformation on the charge and spin degrees of freedom the description of the thermodynamics was possible only in the low-temperature approximation. In the dynamic mean field approximation (DMF), the spins are, as rule, classical [4]. Moreover, the account of kinematic electron contribution presupposes both an infinite space dimension and Dyson's method of diagram summation. In the coherent potential approximation (CPA) [5, 6] the nonzero value of the imaginary part of the Green function on the Fermi level was obtained and the sum rule for spectral density did not hold. One can suppose that evidently the contribution of charge and spin fluctuations was overestimated.

In this paper, the Hamiltonian investigated includes the strong Hund's rule coupling of localized t_{2g} electrons of the Mn^{3+} ion with e_g electrons, superexchange of localized spins, electron–phonon interactions as well as the contributions from phonon subsystem and interaction with the applied magnetic field, h . In the diagrammatic method used the effective self-consistent field is extracted.

The thermodynamics of the DE model with account taken of Hund's rule coupling in the mean field approximation has been previously considered in papers [7–9]. All contributions to the total Green functions in the first nonvanishing approximation with respect to the inverse effective radius of interaction $r \sim 1/z$, where z is the number of nearest neighbour in the simple cubic (s.c.) lattice, were determined.

It should be emphasized that up to now the quantum fluctuations in the effective field theory as applied to manganites have not been taken into account. We have considered all quantum states corresponding to the lower quintet of the zeroth Hund's Hamiltonian, neglecting the influence of the upper triplet. It is valid in the limit of infinite Hund's rule coupling J_H .

The unperturbed Hamiltonian includes the additive part involving the chemical potential and Hund's exchange. In this theory, the Hamiltonian V describing the kinetic electron energy is a perturbation. We suppose that in the system studied the strong electron correlations are realized, and then one can neglect the states with twofold site filling. In a weakly doped electron subsystem with electron concentration $n \sim 1$, the Fermi level lies near the top of the valence band. Then the chemical potential μ is proportional to W , where W is the bandwidth. In this case, the zeroth Hamiltonian, \hat{H}_0 , meets the necessary criteria of the perturbation theory, $\hat{H}_0 \gg V$.

The outline of paper is as follows. In section 2 we write the total Hamiltonian \hat{H} of the Holstein DE model and the diagonalization of unperturbed Hamiltonian \hat{H}_0 is made. Also, we give the unitary transformation of all operators in Hamiltonian \hat{H} . To build the diagrammatic techniques, section 3 presents the main steps including the determination of the free-particle Green functions and rules for pairings in accordance with Wick's theorem. In section 4 the approximate expression for the effective line of interactions is considered. The set of equations for magnetization and chemical potential is derived in section 5. In section 6 we study the spectral and transport properties of this model. The main conclusions are summarized in section 7.

2. The Hamiltonian of the system

In the DE model with electron–phonon interactions the Hamiltonian of the system takes the form

$$\hat{H} = \hat{H}_f + \hat{H}_b, \quad (1)$$

where the Fermi part, \hat{H}_f , is expressed as follows:

$$\hat{H}_f = - \sum_i J_H \mathbf{S}_i \sigma_i - \sum_{i,j} J_{ij} (\mathbf{S}_i + \sigma_i) (\mathbf{S}_j + \sigma_j) - h \sum_i (\mathbf{S}_i^z + \sigma_i^z) - \mu \sum_i n_i + V. \quad (2)$$

The Bohr magneton, μ_B , and \tilde{g} -factor were taken in a unit system with $\mu_B \tilde{g} = 1$. In Hamiltonian (2) the first and second terms describe the Hund's rule coupling and indirect exchange interaction of e_g and t_g electrons, respectively. The next two terms include the interaction of spins with applied magnetic field h and energy of chemical potential μ . For e_g and t_g electrons we can consider the strong one-site Coulomb interaction $U \gg W$ and the kinetic energy of intersite motion. Then we obtain the Heisenberg Hamiltonian in the form similar to the second term of Hamiltonian (2). To have the correct limit when the concentration of e_g electrons $n \rightarrow 1$ corresponding to pure LaMnO_3 , the indirect exchange must also be expressed as in (2).

The perturbation Hamiltonian may be written as

$$\hat{V} = \sum_{i,j,\sigma} t_{ij} c_{\sigma i}^\dagger c_{\sigma j}, \quad (3)$$

where $c_{\sigma i}^\dagger$ ($c_{\sigma i}$) creates (annihilates) an electron of spin σ on lattice site i . This model neglects the e_g orbital degeneracy. The latter plays an important role in both the treatment of the Jahn–Teller effect and the orbital ordering. In LaMnO_3 the e_g bands are split with a gap of order 0.1 eV [10]. Apparently the influence of the upper e_g band is insignificant in the dielectric state at temperatures $T < 500$ K. The boson part of Hamiltonian (1) has a form similar to that used in the theory of a small polaron:

$$\hat{H}_b = -g \sum_i n_i (b_i^\dagger + b_i) + \omega_0 \sum_i b_i^\dagger b_i, \quad (4)$$

where g is the electron–phonon coupling strength, and b_i^\dagger and b_i are the phonon creation and annihilation operators. In the Einstein model the phonon frequency ω_0 is assumed to be dispersion-free.

In the theory proposed, the following relation of parameters, $J_H \gg t_{ij} \sim g \gg |J_{ij}| \sim h$, was used. At first glance the operator V is not the perturbation. However, as will be seen in our further consideration, the hopping integral t_{ij} enters into the expression for the chemical potential μ which is proportional to the bandwidth $W = 2zt$, where t is the nearest-neighbour hopping integral. The zeroth Hamiltonian contains only a part of V , which does not depend on the free carrier concentration. The perturbation near the band half-filling is proportional to the hole concentration, since the electron jumps at $n = 1$ are forbidden for this strongly correlated system. The foregoing provides the basis for the construction of perturbation theory at $n \sim 1$ with the results correct to within $1/z$.

The electron–phonon interactions in manganites were first taken into account in [11], assuming the phonon to be a classical localized oscillator. The main conclusion obtained is that in $\text{La}_{1-x}\text{Sr}_x\text{MnO}_3$ the pure DE model is usable, while in $\text{La}_{1-x}\text{Ca}_x\text{MnO}_3$ the strong electron–phonon interaction plays an essential role.

In the following, the part of Hamiltonian (2) connected with superexchange interaction is considered in the mean-field approximation. We will carry out the unitary transformation $\tilde{U} = \exp(\tilde{S})$ of Hamiltonian (1) resulting in the separation of the fermion and boson operators from each other. The expression for \tilde{S} given by Lang and Firsov [12] has the following form:

$$\tilde{S} = -\frac{gn}{\omega_0} \sum_i (b_i^\dagger - b_i). \quad (5)$$

The shift of Bose

$$\tilde{b} = b + \frac{gn}{\omega_0} \quad (6)$$

and multiplying Fermi operators

$$\tilde{c}_\sigma = Y c_\sigma, \quad (7)$$

where $Y = e^{\lambda(b^\dagger - b)}$ is connected exceptionally with the phonon degree of freedom, $\lambda = g/\omega_0$, results from the transformation \tilde{S} . The Hermitian conjugate of equation (7) is an expression for the creation operator. Substituting the transformed operators in equation (1) we obtain the following zeroth Hamiltonian for the fermion subsystem:

$$\begin{aligned} \hat{H}_{0f} = & \sum_i J_H \mathbf{S}_i \boldsymbol{\sigma}_i - 2J(0) \sum_{ij} (\mathbf{S}_i + \boldsymbol{\sigma}_i) (\langle S_i^z \rangle + \langle \sigma_i^z \rangle) \\ & - \mu \sum_i n_i - h \sum_i (S_i^z + \sigma_i^z) - \xi \sum_i n_i^2, \end{aligned} \quad (8)$$

where $J(0) = zJ$ in the nearest-neighbour approximation, $\xi = g^2/\omega_0$ is the polaron binding energy, and n_i the number of e_g electrons on the i th site. The boson part has the form

$$\hat{H}_{0b} = \omega_0 \sum_i b_i^\dagger b_i. \quad (9)$$

The Hamiltonian of interaction V as a function of c_σ and c_σ^\dagger is expressed in terms of operators \tilde{c}_σ and \tilde{c}_σ^\dagger , respectively.

We will consider the transformed Hamiltonian (1) where the sign of tilde was omitted. Preliminarily we should carry out a diagonalization of Hamiltonian (8) for the Fermi subsystem. The main difficulty is associated with the first term describing Hund's rule coupling between the ion core and the mobile electron. The total basis of the zeroth Fermi Hamiltonian (8) includes 12 spin wavefunctions supposing that the Mn^{4+} ion spin $S = 3/2$ and the e_g electron spin $\sigma = 1/2$. At $h = 0$, in the Hund part of equation (8) the eight spin functions correspond to five- and three-fold degenerated levels of $E_H^0 = -\frac{1}{2}SJ_H$ and $E_H^2 = \frac{1}{2}(S+1)J_H$ with $S_2 = 2$ and $S_1 = 1$ spins, respectively. Spin $S = 3/2$ corresponds to a hole state (Mn^{4+} ion) with the four-fold degenerated energy level of $E_H^1 = 0$. The wavefunctions for the above multiplets are [13]

$$|(3/2, 1/2)S'm\rangle = |\varphi_{S'm}\rangle = \sum_{m_1 m_2} C_{m_1 m_2 m}^{3/2, 1/2, S'} |2m_1, 2m_2\rangle, \quad (10)$$

where $|2m_1, 2m_2\rangle = |3/2, m_1\rangle \otimes |1/2, m_2\rangle$, $C_{m_1 m_2 m}^{3/2, 1/2, S'}$ are the Clebsch–Gordan coefficients. In equation (10), at first, m_2 and then m_1 change from maximum to minimum values. Setting such numeration order the vectors $|2m_1, 2m_2\rangle$ can convert to $|\psi_i\rangle$, where the index $i = 1, 2 \dots 12$. The first five vectors correspond to the quintet E_H^0 , the next three vectors belong to the triplet E_H^2 with electron spin being antiparallel to ion spin, and the last four vectors describe the hole state E_H^1 with spin $S = 3/2$.

Let us introduce the Hubbard operators $X^{ik} = |\psi_i\rangle\langle\psi_k|$. Then the matrix \hat{C} of Clebsch–Gordan coefficients in equation (10) may be presented as

$$\begin{aligned} \hat{C} = & X^{1,1} + X^{5,8} + X^{9,9} + X^{10,10} + X^{11,11} + X^{12,12} + \frac{1}{2}(X^{2,2} + X^{4,7} - X^{6,3} + X^{8,6}) \\ & + \frac{\sqrt{3}}{2}(X^{2,3} + X^{4,6} + X^{6,2} - X^{8,7}) + \frac{1}{\sqrt{2}}(X^{3,4} + X^{3,5} + X^{7,4} - X^{7,5}). \end{aligned} \quad (11)$$

The vector system can be written as

$$|\psi_i\rangle : |3, 1\rangle, |3, -1\rangle, |1, 1\rangle, |1, -1\rangle, |-1, 1\rangle, |-1, -1\rangle, |-3, 1\rangle, |-3, -1\rangle,$$

where $i = 1, 2 \dots 8$, for electron states, and $|\psi_i\rangle : |3, 0\rangle, |1, 0\rangle, |-1, 0\rangle, |-3, 0\rangle$, where $i = 9, 10, 11, 12$ for hole states. The vectors $|\psi_i\rangle$ are connected with eigenfunctions $|\varphi_i\rangle$ of the Hund part in Hamiltonian (8) by the linear relation

$$|\varphi_k\rangle = \sum_i C_{ki} |\psi_i\rangle, \quad (12)$$

where the coefficient C_{ki} forms a matrix \hat{C} in equation (11).

Using the function $|\varphi_k\rangle$, the Hamiltonians (2) and (3) will be transformed. In equation (2), superexchange interaction includes the z -projection of the total spin operator. Then in $|\varphi_k\rangle$ basis, the latter will be presented as a direct sum of diagonal operators $S^z \oplus S_1^z \oplus S_2^z$ for spins $S = 3/2$, $S_1 = 1$ and $S_2 = 2$ [13], respectively. Having constructed a system of Hubbard operators $L^{ik} = |\varphi_i\rangle\langle\varphi_k|$, one can write the unitary transformed zeroth Hamiltonian in the diagonal form:

$$\hat{H}_0 = \sum_{i=1}^N \left\{ \sum_{l=1}^5 \varepsilon_l L_i^{ll} + \sum_{l=9}^{12} \varepsilon_l L_i^{ll} \right\}, \quad (13)$$

where $\tilde{H} = h + 2J(0) ((S^z) + (\sigma^z))$ is the sum of the applied magnetic and effective Weiss fields, $\varepsilon_l = -\frac{1}{2}SJ_H - \mu - \xi - (2S - l)\tilde{H}$ for the state with spin $S_2 = 2$ ($l \leq 5$) and $\varepsilon_l = -(S + 9 - l)\tilde{H}$ for the hole state with $S = 3/2$ ($l \geq 9$). At the same time we have taken into account that $J_H \gg t \gg J$. Therefore the triplet level with $S_1 = 1$ lies considerably above the state with $S_2 = 2$, and can be neglected. We also ignore the contribution of the chemical potential $-\mu(L^{6,6} + L^{7,7} + L^{8,8})$. The above statements can be more strictly proved with the introduction of the projective operator

$$P = \sum_{\alpha=1}^5 L^{\alpha\alpha} + \sum_{\alpha=9}^{12} L^{\alpha\alpha}. \quad (14)$$

The P operator acting upon both the Hamiltonian (1) and wavefunctions to an accuracy of t/J_H eliminates all states with numbers $\alpha = 6, 7$ and 8 .

The operator \mathbf{A} in matrix form can be presented as

$$\mathbf{A} = \sum_{lm} \langle l|A|m\rangle X^{lm}.$$

One can write the following expressions for the electron creation operators:

$$\begin{aligned} c_{\uparrow}^{\dagger} &= X^{1,9} + X^{3,10} + X^{5,11} + X^{7,12} \\ c_{\downarrow}^{\dagger} &= X^{2,9} + X^{4,10} + X^{6,11} + X^{8,12}. \end{aligned} \quad (15)$$

The corresponding formulae for the electron annihilation operators can be obtained using the Hermitian conjugate of equation (15). The Hubbard operators X^{ik} and L^{lm} are related to each other by unitary transformation:

$$X^{ik} = \sum_{lm} C_{li}^* C_{mk} L^{lm}, \quad (16)$$

where the coefficients are determined by the matrix $\hat{\mathbf{C}}$ from equation (11). Substituting (16) in (15) we find the expressions for the unitary transformed $\tilde{c}_{\uparrow}^{\dagger}$ and \tilde{c}_{\uparrow} operators as functions of L^{lm} . An explicit form of both c_{\uparrow}^{\dagger} and c_{\uparrow} operators and electron and ion spin operators is given in the appendix. The operator of the electron number, n , is invariant relative to unitary transformation (12).

3. Fermion–boson free-particle Green function and effective kinematic interaction

In the investigation of electron dynamics we have used the Matsubara Green functions:

$$\mathbf{G}_{\sigma}(\tau, r_l - r_m) = -\langle T_{\tau} c_{l\sigma}(\tau) c_{m\sigma}^{\dagger}(0) \rangle, \quad (17)$$

where T_{τ} is the chronological ordering operator. The operators c_{\uparrow}^{\dagger} and c_{\uparrow} are expressed in the Heisenberg representation. The brackets $\langle \dots \rangle$ mean that the Gibbs thermodynamic average is obtained using the total Hamiltonian (1).

The problem of finding the Green functions reduces to the calculation of various correlators appearing in the scattering matrix series expansion of perturbation theory with Hamiltonian V in interaction representation. Wick's theorem [14, 15] for the Hubbard operators is used for the unlinking of correlators, and then the task reduces to the calculation of elementary Green functions. Every contribution of the perturbation theory has its graphical form. In accordance with equation (7) the free-particle Green functions $U(\tau, \varepsilon_{lm})$ are determined as follows:

$$U(\tau, \varepsilon_{lm}) = -\langle T_\tau Y(\tau)Y(0) \rangle_{0\text{ph}} \langle T_\tau L^{l,m}(\tau)L^{m,l}(0) \rangle_0 \frac{1}{\langle F^{l,m} \rangle_0}, \quad (18)$$

where $\langle F^{l,m} \rangle_0 = \langle L^{l,l} + L^{m,m} \rangle_0$, $\varepsilon_{lm} = \varepsilon_l - \varepsilon_m$. The thermal averages of the first and second correlators in equation (18) are calculated with Hamiltonians (9) and (13), respectively. The Fermi part of equation (18) is easily derived using Wick's theorem:

$$G_{0\text{el}}^{lm}(\tau) = \langle T_\tau L^{l,m}(\tau)L^{m,l}(0) \rangle_0 \frac{(-1)}{\langle F^{l,m} \rangle_0} = e^{\varepsilon_{lm}\tau} \cdot \begin{cases} -f(\varepsilon_{lm}), & \tau > 0 \\ 1 - f(\varepsilon_{lm}), & \tau < 0, \end{cases}$$

where $f(x) = 1/(e^{\beta x} + 1)$ is the Fermi distribution function, and $1/\beta = T$ the temperature.

The Bose part of equation (18) may be determined using both the relation for boson operators b^+ and b , $e^{\lambda(b^\dagger - b)} = e^{-\frac{1}{2}\lambda^2} e^{\lambda b^\dagger} e^{-\lambda b}$, and the Feynman disentangling of the operator products. The detailed calculation is given in [16].

As is seen in equation (18), the Bose part has the form of $G_0^{\text{ph}}(\tau) = \langle T_\tau Y(\tau)Y(0) \rangle_{0\text{ph}} = e^{\Phi(\tau)}$, where

$$\Phi(\tau) = -\lambda^2 \left\{ 2B + 1 - 2\sqrt{B(B+1)} \cosh \left[\omega_0 \left(\tau \mp \frac{\beta}{2} \right) \right] \right\}$$

and the upper minus and the lower plus signs correspond to $\tau > 0$ and $\tau < 0$, respectively. $B = 1/(e^{\beta\omega_0} - 1)$ is the Bose distribution function for the Einstein phonon mode. The appearance of the hyperbolic cosine instead of the ordinary cosine, as in [16], is because in Matsubara's formalism the time t is imaginary, and therefore we must make the substitution $t \rightarrow it$. It is interesting to point out that the function $G_0^{\text{ph}}(\tau)$ describes nondiagonal transitions by the Holstein definition [17], which are responsible for a number of phonons changing in the hopping process. In the function $G_0^{\text{ph}}(\tau)$, the time-independent Debye-Waller factor $e^{-\lambda^2(2B+1)}$ corresponds to diagonal transitions with no changes in the number of virtual phonons.

The Fourier transformation of the single-particle Green function has the form $U(i\omega_n, \varepsilon_{lm}) = \frac{1}{2\beta} \int_{-\beta}^{\beta} U(\tau, \varepsilon_{lm}) e^{i\omega_n \tau} d\tau$. It is easy to write the following relation:

$$e^{x \cosh(z)} = \sum_{k=-\infty}^{\infty} I_k(x) e^{kz},$$

where the $I_k(x)$ are the Bessel functions of the complex argument. Note that in an initial time space we have a simple product of single-particle Green functions of Fermi and Bose subsystems. In Fourier inverse space this relation is complicated:

$$U(i\omega_n, \varepsilon_{lm}) = \frac{1}{\beta} f(\varepsilon_{lm}) e^{-\lambda^2(2B+1)} \sum_{k=-\infty}^{+\infty} I_k(2\lambda^2 \sqrt{B(B+1)}) \frac{e^{\beta\varepsilon_{lm} + \frac{1}{2}\beta k\omega_0} + e^{-\frac{1}{2}\beta k\omega_0}}{i\omega_n + k\omega_0 + \varepsilon_{lm}}, \quad (19)$$

where $\omega_n = \pi(2n + 1)\beta$ and a unit system was taken for $k_B = \hbar = 1$. Since the operators c_σ^\pm and L^{lm} are linearly connected (see equation (A.1) in the appendix) one can write the single-particle Green function as a linear combination of functions $U(i\omega_n, \varepsilon_{lm})$:

$$\begin{aligned} \tilde{G}_{0\sigma}(i\omega_n) = & - \left\{ \left(\delta_{j,0} + \frac{\delta_{j,1}}{4} \right) \langle F^{9,1+j} \rangle_0 U(i\omega_n, \varepsilon_{9,1+j}) + \frac{3-j}{4} \langle F^{10,2+j} \rangle_0 U(i\omega_n, \varepsilon_{10,2+j}) \right. \\ & + \frac{2+j}{4} \langle F^{11,3+j} \rangle_0 U(i\omega_n, \varepsilon_{11,3+j}) \\ & \left. + \left(\frac{\delta_{j,0}}{4} + \delta_{j,1} \right) \langle F^{12,4+j} \rangle_0 U(i\omega_n, \varepsilon_{12,4+j}) \right\}, \end{aligned} \quad (20)$$

where the index $j = 0$ for $\sigma = +1$ (spin up) and $j = 1$ for $\sigma = -1$ (spin down) and $\delta_{i,j}$ is the Kronecker symbol. The identities $\varepsilon_{9,1} = \varepsilon_{10,2} = \varepsilon_{11,3} = \varepsilon_{12,4} = \tilde{\mu} + \frac{1}{2}\tilde{H} = \varepsilon_{0\uparrow}$ and $\varepsilon_{9,2} = \varepsilon_{10,3} = \varepsilon_{11,4} = \varepsilon_{12,5} = \tilde{\mu} - \frac{1}{2}\tilde{H} = \varepsilon_{0\downarrow}$ are valid, where $\tilde{\mu} = \mu + \xi + \frac{1}{2}SJ_H$. Here the change of electron energy with spin σ transferring from site to site is denoted by $\varepsilon_{0\sigma}$. Then expression (20) is simplified and takes the form

$$\tilde{G}_{0\sigma}(i\omega_n) = \langle F^{\sigma 0} \rangle_0 G_{0\sigma}(i\omega_n) = \langle F^{\sigma 0} \rangle_0 U(i\omega_n, \varepsilon_{0\sigma}), \quad (21)$$

where a combined occupancy of electron-hole states $\langle F^{\sigma 0} \rangle_0$ in the mean-field approximation is defined as

$$\begin{aligned} \langle F^{+0}(\varepsilon_1, \varepsilon_2, \varepsilon_3, \varepsilon_4, \varepsilon_5, \varepsilon_9, \varepsilon_{10}, \varepsilon_{11}, \varepsilon_{12}) \rangle_0 &= \langle F^{9,1} \rangle_0 + \frac{3}{4} \langle F^{10,2} \rangle_0 + \frac{1}{2} \langle F^{11,3} \rangle_0 + \frac{1}{4} \langle F^{12,4} \rangle_0 \\ \langle F^{-0}(\varepsilon_1, \varepsilon_2, \varepsilon_3, \varepsilon_4, \varepsilon_5, \varepsilon_9, \varepsilon_{10}, \varepsilon_{11}, \varepsilon_{12}) \rangle_0 &= \frac{1}{4} \langle F^{9,2} \rangle_0 + \frac{1}{2} \langle F^{10,3} \rangle_0 + \frac{3}{4} \langle F^{11,4} \rangle_0 + \langle F^{12,5} \rangle_0. \end{aligned} \quad (22)$$

For the sake of convenience we have written $\langle F^{\sigma 0} \rangle_0$ as a function of all energy parameters ε_l . It can be shown that expression (21) coincides with the unperturbed Green function given in [6]. The equality

$$F^{\sigma 0} = n_\sigma + p_\sigma, \quad (23)$$

where n_σ and p_σ are the operators of number of electrons and holes with spin σ expressed in terms of L^{lm} (see the appendix), will be further used. Using the equalities of ((A.2)–(A.4)) in the appendix, equation (23) can be written as

$$\langle F^{\sigma 0} \rangle = \frac{1}{8}(5 - n) + \sigma \langle \sigma^z + \frac{1}{4}S_0^z \rangle, \quad (24)$$

where $S_0^z = \frac{3}{2}(L^{9,9} - L^{12,12}) + \frac{1}{2}(L^{10,10} - L^{11,11})$ is the z -projection of spin in basis of t_{2g} electrons as in the Mn^{4+} ion. It is easy to check that the expectations of operators $\langle \sigma^z + \frac{1}{4}S_0^z \rangle$ and $\frac{1}{4}\langle \sigma^z + S^z \rangle$ are equal (see the appendix). Thus, a quarter of the Mn^{4+} ion spin fluctuates with the electron spins. The reason is that the Mn^{4+} ion spins are coupled to the spins of an itinerant e_g -electron not only by Hund's exchange but by effective kinematic interaction as well. This point of view will be confirmed in the following discussion.

We will formulate some rules to find the contributions of a series of perturbation theory in both Green function and combined occupancies using a graphic representation. In figures 1 and 2, the electron Green functions $G_{0\sigma}(i\omega_n)$, $G_{+-}(i\omega_n) = U(i\omega_n, \varepsilon_{\uparrow\downarrow})$ and Fourier components of the interaction

$$t(\mathbf{q}) = \sum_{ij} t_{ij} e^{-i\mathbf{q}(\mathbf{r}_i - \mathbf{r}_j)} = 2t(\cos(q_x a) + \cos(q_y a) + \cos(q_z a)),$$

where $\varepsilon_{\uparrow\downarrow} = \varepsilon_{0\downarrow} - \varepsilon_{0\uparrow}$ and a is the constant of the s.c. lattice, are presented by solid, dashed and wavelines, respectively.

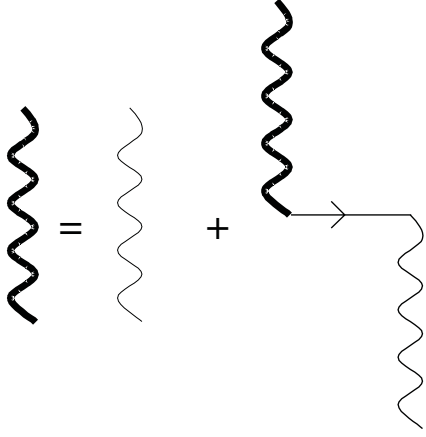


Figure 1. Graphic equation for effective kinematic interaction.

Using Wick's theorem one can write all possible pairings realized in the framework of this consideration. The c_σ operators and new Bose operator $B^+ = \sigma^+ + \frac{1}{2}S_0^+$ are 'active' operators where

$$S_0^+ = \frac{\sqrt{3}}{2}(L^{9,10} + L^{11,12}) + L^{10,11},$$

$$\sigma^+ = \frac{1}{2}(L^{1,2} + L^{4,5}) + \sqrt{\frac{3}{8}}(L^{2,3} + L^{3,4}).$$

The operators B^- and σ^- appear due to the Hermitian conjugate of B^+ and σ^+ operators, respectively ($B^- = (B^+)^+$, $\sigma^- = (\sigma^+)^+$). We have the following zero pairings:

$$(n_{\sigma i} + p_{\sigma i}) \underset{\leftarrow}{c_{\sigma j}} = c_{\sigma_1 i} \underset{\leftarrow}{c_{\sigma_2 j}} = c_{\sigma_1 i}^\dagger \underset{\leftarrow}{c_{\sigma_2 i}^\dagger} = B_i^\sigma \underset{\leftarrow}{c_{\bar{\sigma} j}} = 0. \quad (25)$$

Here i and j site symbols mean the time indices in the interaction representation. In pairings the arrows are directed from 'active' to 'passive' operators. The remaining nonzero pairings have the form

$$(n_{\sigma i} + p_{\sigma i}) \underset{\leftarrow}{c_{\bar{\sigma} j}} = \frac{1}{4}\delta_{ij}G_{0\bar{\sigma}}(\tau_j - \tau_i)c_{\bar{\sigma} i}, \quad c_{\sigma i}^\dagger \underset{\leftarrow}{c_{\bar{\sigma} j}} = \delta_{ij}G_{0\bar{\sigma}}(\tau_j - \tau_i)B_i^\sigma$$

$$B_i^\sigma \underset{\leftarrow}{c_{\sigma j}} = -\frac{1}{4}\delta_{ij}G_{0\sigma}(\tau_j - \tau_i)c_{\bar{\sigma} i}, \quad \left(\sigma_i^z + \frac{1}{4}S_{0i}^z\right) \underset{\leftarrow}{c_{\sigma j}} = -\frac{\sigma}{8}\delta_{ij}G_{0\sigma}(\tau_j - \tau_i)c_{\sigma i}$$

$$(n_{\sigma i} + p_{\sigma i}) \underset{\leftarrow}{B_j^+} = \frac{\sigma}{4}\delta_{ij}G_{+-}(\tau_j - \tau_i)B_i^+, \quad B_i^- \underset{\leftarrow}{B_j^+} = -\frac{1}{2}\delta_{ij}G_{+-}(\tau_j - \tau_i)(\sigma_i^z + \frac{1}{4}S_{0i}^z). \quad (26)$$

The presented expressions are closed and allow us to find the contribution of a series of perturbation theory using only three single-particle Green functions in spite of the existence of a large number of Hubbard operators L^{ik} . This result is important and essentially simplifies the construction of diagram techniques in the DE model with a strong Hund's rule coupling.

Let us find an analytic expression for the effective kinematic interactions $\beta B_{\sigma^+ c_\sigma}(\mathbf{q}, i\omega_n)$ displayed by the bold line in figure 1. This expression may be written as

$$\beta B_{\sigma^+ c_\sigma}(\mathbf{q}, i\omega_n) = \frac{\beta t(\mathbf{q})}{1 - \beta t(\mathbf{q})G_{0\sigma}(i\omega_n)\langle F^{\sigma 0} \rangle}. \quad (27)$$

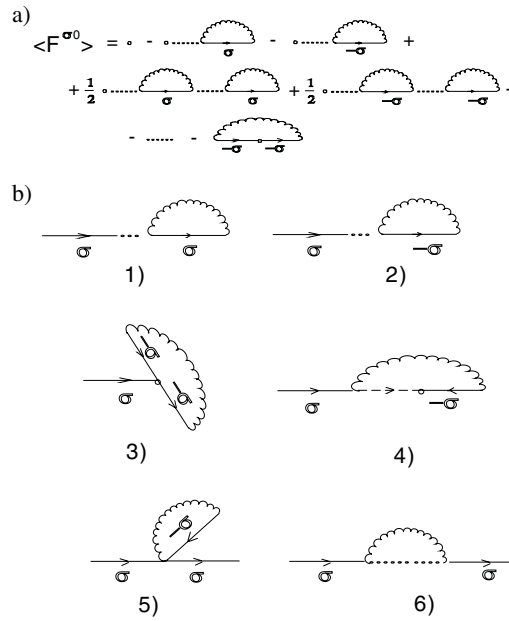


Figure 2. Graphic image of the equation for combined occupancy ($F^{\sigma 0}$) (a) and diagrams for the Green function in the first approximation of the perturbation theory (b).

In the absence of electron–phonon interaction the calculation of diagrams presents no problems [8]. In this case, equation (27) has the simplest form:

$$\beta B_{\sigma}^{c_{\sigma}^{\dagger} c_{\sigma}}(\mathbf{q}, i\omega_n) = \frac{\beta t(\mathbf{q})(i\omega_n + \varepsilon_{0\sigma})}{i\omega_n - E_{\sigma\mathbf{q}}}, \quad (28)$$

where $E_{\sigma\mathbf{q}} = -\varepsilon_{0\sigma} + t(\mathbf{q})\langle F^{\sigma 0} \rangle$.

If equation (28) contains one pole, the infinite quantity of poles in equation (27) are the solutions of an algebraic equation of infinite order. As a consequence, there is an unlimited quantum number of phonons. With the aim of practical use, equation (27) should be simplified.

4. Electron–phonon interaction

In the CPA method [6] the polaron problem is considerably simplified after analytic continuation $i\omega_n \rightarrow \omega + i\delta$ and use of a self-consistent equation for the total Green function $G_{\sigma}(\omega, 0) = U(\omega - \frac{W^2}{16}G_{\sigma}(\omega, 0), \varepsilon_{0\sigma})$. Writing $G_{\sigma}(\omega, 0)$ as a sum of real and imaginary parts, it is easy to solve the derived set of equations by a simple iteration method.

Let us consider the next approximations in solving equation (27) for frequency poles. The equation of pole singularities for the effective kinematic interaction (27) is written in the form

$$\prod_m (x + m\omega_0) - t(\mathbf{q})\langle F^{\sigma 0} \rangle P_{\sigma} \sum_m \varphi_{m\sigma} \prod_{k(\neq m)} (x + k\omega_0) = 0, \quad (29)$$

where

$$x = i\omega_n + \varepsilon_{0\sigma} \quad P_{\sigma} = f(\varepsilon_{0\sigma})e^{-\lambda^2(2B+1)},$$

$$\varphi_{m\sigma} = I_m(2\lambda^2\sqrt{B(B+1)})(e^{\beta[\varepsilon_{0\sigma} + \frac{1}{2}m\omega_0]} + e^{-\frac{1}{2}\beta m\omega_0}).$$

The second term in equation (29) is considered as a perturbation. It is correct in the limit of strong electron–phonon coupling, when $P_\sigma \varphi_{m\sigma} \ll 1$. In the case of $g = 0$, using equation (29) we obtain the solution corresponding to the DE model. In equation (29) the term with $m = 0$ corresponds to the central polaron band. Expressing the n th root of equation (29) as $x = x_n + \Delta_n$, where $x_n = -n\omega_0$ is the root in the absence of perturbation, it is easy to calculate a correction to the n th pole in the linear approximation relative to the smallness of the $P_\sigma \varphi_{m\sigma}$ parameter:

$$\Delta_n = t(\mathbf{q}) \langle F^{\sigma 0} \rangle P_\sigma \varphi_{n\sigma}. \quad (30)$$

Then one can write equation (27) accurate to $t(q)^2$ as

$$\begin{aligned} \beta B_{\sigma^* c_\sigma}(\mathbf{q}, i\omega_n) &= \beta t(\mathbf{q}) \prod_m \frac{i\omega_n + \varepsilon_{0\sigma} + m\omega_0}{(i\omega_n - E_{m\sigma\mathbf{q}})} \\ &\approx \beta t(\mathbf{q}) \left\{ 1 + t(\mathbf{q}) \langle F^{\sigma 0} \rangle P_\sigma \sum_{m=-\infty}^{\infty} \frac{\varphi_{m\sigma}}{i\omega_n - E_{m\sigma\mathbf{q}}} \right\} \end{aligned} \quad (31)$$

where $E_{m\sigma\mathbf{q}} = -\varepsilon_{0\sigma} - m\omega_0 + t(\mathbf{q}) \langle F^{\sigma 0} \rangle P_\sigma \varphi_{m\sigma}$.

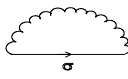
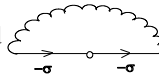
5. The analysis of magnetic structure

Using the approximations (31) for the effective kinematic interaction, we will write the system of equations determining the chemical potential and mean spin of the system. The graphic image of a series expansion for combined occupancies $\langle F^{\sigma 0} \rangle$ is presented in figure 2(a). A small circle \circ corresponds to $\langle F_i^{\sigma 0} \rangle_0$ of the i th site. The lower index for $\langle F_i^{\sigma 0} \rangle_0$ denotes the averaging over Hamiltonian \hat{H}_0 (equation (13)) with the parametric part tending to zero:

$$\hat{H}_0(r_\uparrow, r_\downarrow) = \hat{H}_0 + \sum_i^N (r_{\uparrow i} F_i^{+0} + r_{\downarrow i} F_i^{-0}). \quad (32)$$

The dots connecting the diagram blocks (figure 2) mean the equality of their external site indices. According to the linked cluster theorem such diagrams characterize the contributions to both combined occupancies and Green function. The form of the zeroth Hamiltonian (32) is very suitable for calculation of the operator average:

$$\langle F_i^{\sigma 0} \rangle_0 = \frac{\partial}{\partial (-\beta r_{\sigma i})} \ln \text{Tr}(\exp(-\beta \hat{H}_0(r_\uparrow, r_\downarrow))) = \partial_\sigma \ln Z_0(r_\uparrow, r_\downarrow). \quad (33)$$

In figure 2 the blocks  and  are described by the functions $\beta \delta \mu_\sigma$ and $\nu_{-\sigma} \langle F^{-\sigma 0} \rangle$:

$$\begin{aligned} \delta \mu_\sigma &= \frac{1}{N} \sum_{\mathbf{q}} t(\mathbf{q}) P_\sigma \sum_{m=-\infty}^{\infty} \varphi_{m\sigma} f(E_{m\sigma\mathbf{q}}) \\ \nu_{-\sigma} \langle F^{-\sigma 0} \rangle &= \frac{1}{N} \sum_{\mathbf{q}} P_\sigma \sum_{m=-\infty}^{\infty} \varphi_{m\sigma} (f(E_{m\sigma\mathbf{q}}) - f(-m\omega_0 - \varepsilon_{0\sigma})). \end{aligned} \quad (34)$$

In the sums of equation (34) the m_1 and m_2 indices were taken equal to m , since otherwise the corresponding series terms are proportional to a high-order power of the parameter $P_\sigma \varphi_{m\sigma}$.

In figure 2(a), graphic series may be easily summed, since all terms of the sum with the exception of the last one $\nu_{-\sigma} \langle F^{-\sigma 0} \rangle$ generate the Taylor power series

$$\begin{aligned} \langle F^{\sigma 0} \rangle_0 - \partial_\sigma \langle F^{\sigma 0} \rangle_0 \beta \delta \mu_\sigma - \partial_{-\sigma} \langle F^{-\sigma 0} \rangle_0 \beta \delta \mu_{-\sigma} \\ + \frac{1}{2!} \partial_\sigma^2 \langle F^{\sigma 0} \rangle_0 (\beta \delta \mu_\sigma)^2 + \frac{1}{2!} \partial_{-\sigma}^2 \langle F^{-\sigma 0} \rangle_0 (\beta \delta \mu_{-\sigma})^2 - \dots, \end{aligned}$$

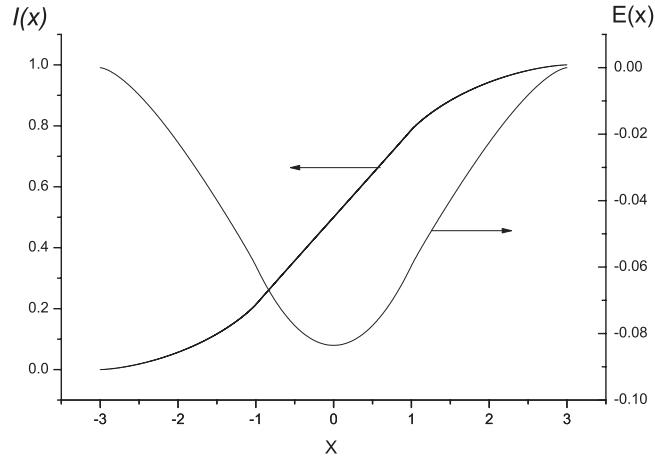


Figure 3. $I(x)$ and $E(x)$ functions.

the sum of which is equal to $\langle F^{\sigma 0} \rangle_1$:

$$\langle F^{\sigma 0} \rangle_1 = \langle F^{\sigma 0}(\tilde{\varepsilon}_1, \tilde{\varepsilon}_2, \tilde{\varepsilon}_3, \tilde{\varepsilon}_4, \tilde{\varepsilon}_5, \tilde{\varepsilon}_9, \tilde{\varepsilon}_{10}, \tilde{\varepsilon}_{11}, \tilde{\varepsilon}_{12}) \rangle_0. \quad (35)$$

The function $\langle F^{\sigma 0}(\varepsilon_1, \varepsilon_2, \varepsilon_3, \varepsilon_4, \varepsilon_5, \varepsilon_9, \varepsilon_{10}, \varepsilon_{11}, \varepsilon_{12}) \rangle_0$ is determined by equation (22) and

$$\begin{aligned} \tilde{\varepsilon}_1 &= \varepsilon_1 + \delta\mu_{\uparrow}, & \tilde{\varepsilon}_2 &= \varepsilon_2 + \frac{3}{4}\delta\mu_{\uparrow} + \frac{1}{4}\delta\mu_{\downarrow}, \\ \tilde{\varepsilon}_3 &= \varepsilon_2 + \frac{1}{2}(\delta\mu_{\uparrow} + \delta\mu_{\downarrow}), & \tilde{\varepsilon}_4 &= \varepsilon_4 + \frac{1}{4}\delta\mu_{\uparrow} + \frac{3}{4}\delta\mu_{\downarrow}, \\ \tilde{\varepsilon}_5 &= \varepsilon_5 + \delta\mu_{\downarrow}, & \tilde{\varepsilon}_9 &= \varepsilon_9 + \delta\mu_{\uparrow} + \frac{1}{4}\delta\mu_{\downarrow}, \\ \tilde{\varepsilon}_{10} &= \varepsilon_{10} + \frac{3}{4}\delta\mu_{\uparrow} + \frac{1}{2}\delta\mu_{\downarrow}, & \tilde{\varepsilon}_{11} &= \varepsilon_{11} + \frac{1}{2}\delta\mu_{\uparrow} + \frac{3}{4}\delta\mu_{\downarrow}, \\ \tilde{\varepsilon}_{12} &= \varepsilon_{12} + \frac{1}{4}\delta\mu_{\uparrow} + \delta\mu_{\downarrow}. \end{aligned}$$

Equations for the mean spin $\langle \sigma^z + \frac{1}{4}S_0^z \rangle$ as well as for the chemical potential μ can be written in the following form:

$$\begin{aligned} \frac{1}{8}(5-n) + \langle \sigma^z + \frac{1}{4}S_0^z \rangle &= \langle F^{+0} \rangle_1 - \nu_1 \langle F^{-0} \rangle \\ \frac{1}{8}(5-n) - \langle \sigma^z + \frac{1}{4}S_0^z \rangle &= \langle F^{-0} \rangle_1 - \nu_1 \langle F^{+0} \rangle. \end{aligned} \quad (36)$$

We will consider the different solutions of the set of equations (36). Supposing that $\xi = 0$, $T = 0$ (pure double exchange) and $\mu > 0$, we introduce the functions $E(x) = \frac{1}{6} \int_{-3}^x D_c(y) y dy$ and $I(x) = \int_{-3}^x D_c(y) dy$, where the electron density of states may be written as

$$D_c(x) = \frac{1}{N} \sum_{\mathbf{q}} \delta\left(x - \frac{t(\mathbf{q})}{2t}\right). \quad (37)$$

Here $\delta(x)$ is the Dirac delta function. From equation (37) it follows that for a simple cubic (s.c.) lattice the variable $|x| \leq 3$. The plots of $I(x)$ and $E(x)$ functions for this lattice are displayed in figure 3. Function $E(x)$ characterizes an effective field contribution to the electron dynamics which does not exceed $1/(2z)$. This contribution roughly determines the Curie temperature, T_C , in units of the bandwidth W .

For the case of $\langle F^{+0} \rangle_1 = 1$, $\langle F^{-0} \rangle_1 = 0$, the set of equations (36) can be written as

$$\langle F^{\sigma 0} \rangle = \langle F^{\sigma 0} \rangle_1 + \frac{1}{4} \left[1 - I\left(\frac{6\mu}{W \langle F^{-\sigma 0} \rangle}\right) \right], \quad (38)$$

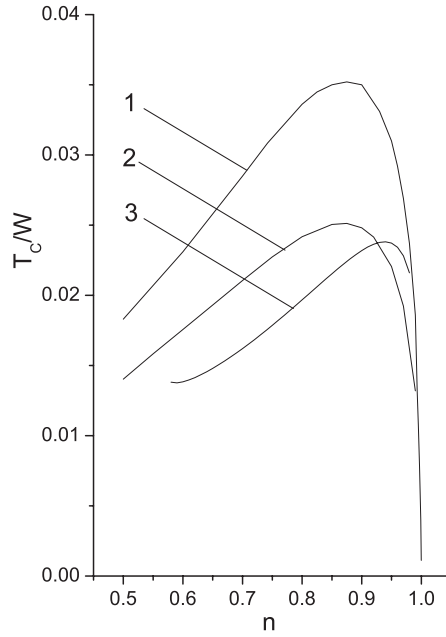


Figure 4. The Curie temperature, T_C , versus electron concentration, n , with account of Hund's rule coupling in the framework of given theory (curve 1), and in the mean-field approximation [9] (curve 2). Curve (3) corresponds to an approximate solution of the set of equations (41).

which have solutions if

$$\frac{6\mu}{W\langle F^{-0} \rangle} \geq 3. \quad (39)$$

Then the expressions for both the mean spin of a saturated ferromagnet (FM) and the chemical potential have the form $\langle \sigma^z + \frac{1}{4}S_0^z \rangle = \frac{1}{8}(3+n)$ and $\frac{\tilde{\mu}}{W} = \frac{1}{6}I^{-1}(n)$, respectively, where $I^{-1}(x)$ is the inverse function of $I(x)$. In figure 3 it is seen that $I^{-1}(x) > 0$ for $x > 0.5$. Therefore, the self-consistent FM solution is valid for electron concentrations $n > 1/2$. In perovskite manganites this fact was fixed experimentally in [18]. Using equation (39) we obtain a more precise estimation of electron concentration, namely, $n_{\text{FM}} \approx 0.588$, above which the FM state exists.

The set of equations (36) has solutions $\langle \sigma^z + \frac{1}{4}S_0^z \rangle = 0$, $\tilde{\mu} = \tilde{\mu}_{\text{PM2}} = \frac{W}{48}(5-n)I^{-1}(\frac{n+1}{2})$ and $\tilde{\mu} = \tilde{\mu}_{\text{PM1}} = \frac{W}{48}(5-n)I^{-1}(\frac{n}{2})$, corresponding to two paramagnetic phases PM-2 and PM-1. In these phases $\langle F^{\sigma 0} \rangle_1 = 1/2$, $\tilde{\mu} + \delta\mu_{\sigma}/4 > 0$ and $\langle F^{\sigma 0} \rangle_1 = 5/8$, $\tilde{\mu} + \delta\mu_{\sigma}/4 < 0$, respectively. The existence of two paramagnetic phases was also predicted in [8] for high-temperature superconducting systems.

To find the temperature T_C the set of equations in the linear approximation is expanded in terms of the small parameter $\langle \sigma^z + \frac{1}{4}S_0^z \rangle$ at $T \sim T_C$. Neglecting superexchange and supposing $\xi = 0$ (pure DE model) we obtain the following equations for μ and T_C :

$$1 - n = \frac{1}{1 + \frac{5}{4}e^{\beta_C(\tilde{\mu} + \frac{1}{4}\delta\mu)}} - \frac{2}{N} \sum_{\mathbf{q}} f(E_{0\mathbf{q}}) + 2f(-\tilde{\mu}) \quad (40)$$

$$4T_C^2 = \frac{1}{N} \sum_{\mathbf{q}} t(\mathbf{q})f(E_{0\mathbf{q}})[1 - f(E_{0\mathbf{q}})] \left\{ 5t(\mathbf{q}) \frac{e^{\beta_C(\tilde{\mu} + \frac{1}{4}\delta\mu)} + \frac{1}{2}}{5e^{\beta_C(\tilde{\mu} + \frac{1}{4}\delta\mu)} + 4} - T_C \right\},$$

where $\beta_C = 1/T_C$, $\delta\mu = \frac{1}{N} \sum_{\mathbf{q}} t(\mathbf{q})f(E_{0\mathbf{q}})$, $E_{0\mathbf{q}} = -\tilde{\mu} + \frac{1}{8}(5-n)t(\mathbf{q})$.

The results of $T_C(n)$ calculation in W units are shown in figure 4 (curve 1). The dependence $T_C(n)$ obtained assuming that $\tilde{\mu} = \tilde{\mu}_{PM2}$ (see the above formula for the chemical potential defined at $T = 0$) and $\frac{df(E_{0q})}{dE_{0q}} = -\delta(E_{0q})$ has the form

$$T_C/W \approx \frac{768(\tilde{\mu}/W)^2 D_c \left(\frac{48\tilde{\mu}/W}{5-n} \right)}{[(5-n)^3 + 384(5-n) D_c \left(\frac{48\tilde{\mu}/W}{5-n} \right) \tilde{\mu}/W]}. \quad (41)$$

Formula (41) differs somewhat from the result obtained in [9], when the Hund's rule coupling was considered in the mean-field approximation (see curve 2 in figure 4). Curve 3 corresponds to a solution of the set of equations (40). Therefore, one can note that a rigorous account of quantum spin fluctuation decreases the Curie temperature significantly (up to 30%).

The above equations correspond to a pure DE model. There are no difficulties in the derivation of similar formulae taking into account the strong electron–phonon coupling. As is seen in the approximation (equation (34)) the strong influence of the polaron binding energy ξ on the ferromagnetic phase is observed. The temperature dependences of mean spin obtained solving the set of equations (36) at electron concentration $n = 0.8$ for various values of ξ are illustrated in figure 5. Hereinafter the phonon frequency value $\omega_0/W = 0.025$ and the lattice constant $a = 5 \text{ \AA}$ were used. It is seen that the Curie temperature is reduced by more than a half at $\xi/W = 0.04$. The chemical potential also decreases abruptly. This is indicative of a narrowing effective band. The size of the polaron calculated using the Holstein expression $aW/\xi \approx 25a$ is not small. Therefore, the electron–phonon interaction suppresses the DE interaction, as predicted in [6, 11].

6. Spectral and transport properties of electron–hole excitations

In figure 2(b), all diagrams in the first order relative to the inverse effective radius of interaction for the Green function $G_\sigma(i\omega_n, \mathbf{k})$ are shown. Diagrams 1, 2, 3 and those in a higher order of expansion forming a series $\langle F^{\sigma 0} \rangle$ are depicted in figure 2(a). Consequently, the appropriate correction to $G_\sigma(i\omega_n, \mathbf{k})$ is equal to $\langle F^{\sigma 0} \rangle G_{0\sigma}(i\omega_n)$.

Let us write the analytic expressions for diagrams 4, 5 and 6 for strong electron–phonon interaction:

$$\begin{aligned} \Lambda_4^\sigma(i\omega_n) &= \frac{\sigma}{2N} \sum_{\mathbf{qm}} \frac{t(\mathbf{q}) P_{-\sigma} \varphi_{m-\sigma} P_0 \varphi_{00}}{i\omega_n - E_{m-\sigma\mathbf{q}} + \varepsilon_{-\sigma\sigma}} \{f(E_{m-\sigma\mathbf{q}}) + b(\varepsilon_{-\sigma\sigma})\} \left\langle \sigma^z + \frac{1}{4} S_0^z \right\rangle_0 \\ \Delta_5^\sigma &= -\frac{1}{4} \beta \delta \mu_{-\sigma} \langle F^{\sigma 0} \rangle \\ \Delta_6^\sigma(i\omega_n) &= \frac{1}{N} \sum_{\mathbf{qm}} \frac{\beta t^2(\mathbf{q}) \langle F^{\sigma 0} \rangle P_\sigma \varphi_{m\sigma}}{i\omega_n - E_{m\sigma\mathbf{q}}} \langle F_p^{\sigma 0} F_l^{\sigma 0} \rangle_0. \end{aligned} \quad (42)$$

Here, $b(x) = 1/(\exp(\beta x) - 1)$ is the Bose distribution function, $P_0 \varphi_{00} = e^{-\lambda^2(2B+1)} I_0(2\lambda^2 \sqrt{B(B+1)})$, $\langle \sigma^z + \frac{1}{4} S_0^z \rangle_0 \approx \frac{5}{4} \beta \tilde{H} \frac{2e^{\beta\tilde{\mu}} + 1}{5e^{\beta\tilde{\mu}} + 4}$. Since $\beta \tilde{H} \ll 1$, the nonzero contribution to $\Lambda_4^\sigma(i\omega_n)$ is proportional to $b(\varepsilon_{-\sigma\sigma}) \langle \sigma^z + \frac{1}{4} S_0^z \rangle_0 \approx \frac{1}{2\sigma}$ at $\beta \tilde{\mu} \gg 1$. Also, for linked diagrams which are proportional to δ_{pl} we have $\langle F_p^{\sigma 0} F_l^{\sigma 0} \rangle_0 = m(\tilde{\mu}) \delta_{pl}$, where $m(\tilde{\mu}) = \frac{5}{8} \frac{(5e^{\beta\tilde{\mu}} + 2)(e^{\beta\tilde{\mu}} + 1)}{(5e^{\beta\tilde{\mu}} + 4)^2}$.

To find the final expressions for the diagrams, the value of $\Lambda_4^\sigma(i\omega_n)$ should be multiplied by $G_{0\sigma}(i\omega_n)$ and Δ_5^σ and Δ_6^σ by $G_{0\sigma}(i\omega_n)^2$. Then the self-energy $\sum_\sigma(i\omega_n)$ is written as

$$\sum_\sigma(i\omega_n) = \langle F^{\sigma 0} \rangle G_{0\sigma}(i\omega_n) + \Lambda_4^\sigma(i\omega_n) G_{0\sigma}(i\omega_n) + (\Delta_5^\sigma + \Delta_6^\sigma(i\omega_n)) G_{0\sigma}(i\omega_n)^2. \quad (43)$$

Using the Larkin equation [19] the total Green function $G_\sigma(i\omega_n, \mathbf{k})$ can be easily found:

$$G_\sigma(i\omega_n, \mathbf{k}) = \frac{\sum_\sigma(i\omega_n)}{1 - \beta t(\mathbf{k}) \sum_\sigma(i\omega_n)}. \quad (44)$$

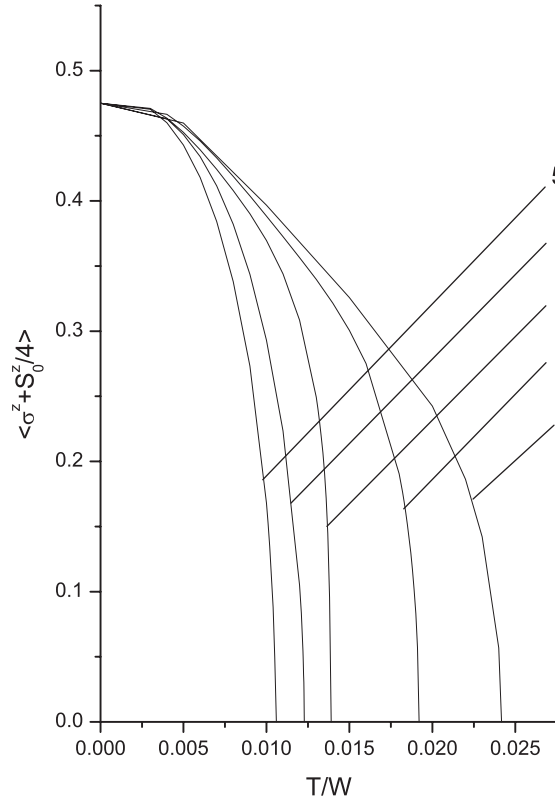


Figure 5. Temperature dependences of magnetization $\langle \sigma^z + \frac{1}{4}S_0^z \rangle$ for $n = 0.8$ with $\xi/W = 0, 0.003, 0.01, 0.03$ and 0.04 (curves 1–5, respectively).

In the DE model ($\xi = 0$) this formula is essentially simplified:

$$G_\sigma(i\omega_n, \mathbf{k}) = \frac{1}{\beta} \frac{\langle F^{\sigma 0} \rangle + \Lambda_4^\sigma(i\omega_n)}{i\omega_n - \omega_{\sigma \mathbf{k}}}, \quad (45)$$

where $\omega_{\sigma \mathbf{k}} = -\varepsilon_{0\sigma} - \frac{1}{4}\delta\mu_{-\sigma} + (\langle F^{\sigma 0} \rangle + \Lambda_4^\sigma(i\omega_n))t(\mathbf{k}) + \frac{\Delta_6^\sigma(i\omega_n)}{\beta \langle F^{\sigma 0} \rangle}$.

To deduce equation (45) we have used the linear expansion of small parameters. Realizing in equations (44) and (45) an analytical continuation $i\omega_n \rightarrow \omega + i\delta$ we obtain a retarded Green function, the poles of which determine the $\Omega(\mathbf{k})$ spectrum of excitations. The imaginary part $G_\sigma(i\omega_n, \mathbf{k})$ determines the spectral density being proportional to $\delta(\omega - \Omega(\mathbf{k}))$ for coherent excitations.

The spectral density of the incoherent spectrum describing the relaxation processes is of principal interest. After analytical continuation $i\omega_n \rightarrow \omega + i\delta$ using equations (42) one can evaluate the nonzero imaginary parts of $\Lambda_4^\sigma(\Omega(\mathbf{k}))$ and $\Delta_6^\sigma(\Omega(\mathbf{k}))$. The corresponding formulae are given in the appendix (equations (A.5) and (A.6)). $\sum'_\sigma(\omega)$ and $\sum''_\sigma(\omega)$ correspond to the real and imaginary parts of the self-energy $\sum_\sigma(\omega)$, respectively. Let us write the imaginary part $\text{Im}(G_\sigma(i\omega_n, \mathbf{k}))$ of the total Green function as

$$\text{Im}(G_\sigma(\omega + i\delta, \mathbf{k})) = \frac{\sum''_\sigma(\omega)}{(1 - \beta t(\mathbf{k}) \sum'_\sigma(\omega))^2 + (\beta t(\mathbf{k}) \sum''_\sigma(\omega))^2}. \quad (46)$$

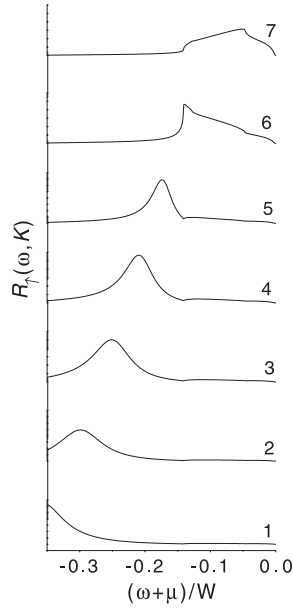


Figure 6. Frequency dependence of spectral density for the up-spin band in the FM phase at $n = 0.8$, $\xi = 0$, $T/W = 0.02$ and $t(\mathbf{q})/W = -0.4, -0.35, -0.3, -0.25, -0.2, -0.1$ and -0.05 (curves 1–7, respectively).

In the case of incoherent excitations the spectral density $R_\sigma(\omega, \mathbf{k}) = -2\beta \text{Im}(\mathbf{G}_\sigma(\omega + i\delta, \mathbf{k}))$ will be different from zero over a certain frequency interval in which the electron density of state $D_C(x)$ also has nonzero value.

In figure 6 the frequency dependences of the spectral density, $R_\uparrow(\omega, \mathbf{k})$, for the up-spin band in the FM phase ($T_C/W = 0.024$) are shown at $\xi = 0$, $T/W = 0.02$ ($\mu/W = 0.147$) and $n = 0.8$. The curves 1–7 display the shift of maximum $R_\uparrow(\omega, \mathbf{k})$ towards the Fermi energy $\omega = -\mu$ with increasing $t(\mathbf{q})/W$ from -0.4 to -0.05 , respectively. We have a similar behaviour of $R_\uparrow(\omega, \mathbf{k})$ with decreasing T . When this result is compared with APRES spectra (see figure 2a in [20]), it is apparent that there is qualitative agreement between theory and experiment. The same result was obtained in the CPA method [21]. After the replacement $t(q) \rightarrow -t(q)$ the figure changes symmetrically about $\omega = -\mu$. It should be emphasized that in this theory $R_\sigma(-\tilde{\mu}, \mathbf{k}) = 0$.

Figure 7 displays the frequency dependence of the spectral density $R_\sigma(\omega, \vec{k})$ in the approximation (31) for the effective line at $n = 0.8$, $\xi/W = 0.03$ and $t(\mathbf{q})/W = 1/3$. Curves 1 and 2 correspond to up- and down-spin bands at low temperature ($T/W = 0.005$) and curve 3 to the PM-2 phase. As in figure 6, for the incoherent spectrum of excitations the spectral density $R_\sigma(\omega, \vec{k})$ in the FM state has a broad maximum. It is seen that very sharp peaks characteristic of coherent polaron excitation only occur in the PM-2 phase (see the inset in figure 7). Therefore polarons are involved in the conductivity above the temperature T_C , and increase it. In experiments, the coherent peaks are difficult to observe because of polaron scattering. Unfortunately, the value $\rho(T)$ near T_C (in the PM phase) does not exceed a few $\text{m}\Omega \text{ cm}$, which is inconsistent with the experiment. Seemingly, near the phase transition the vertex corrections in the Green function begin to play an important role. This problem is very complicated and demands special consideration.

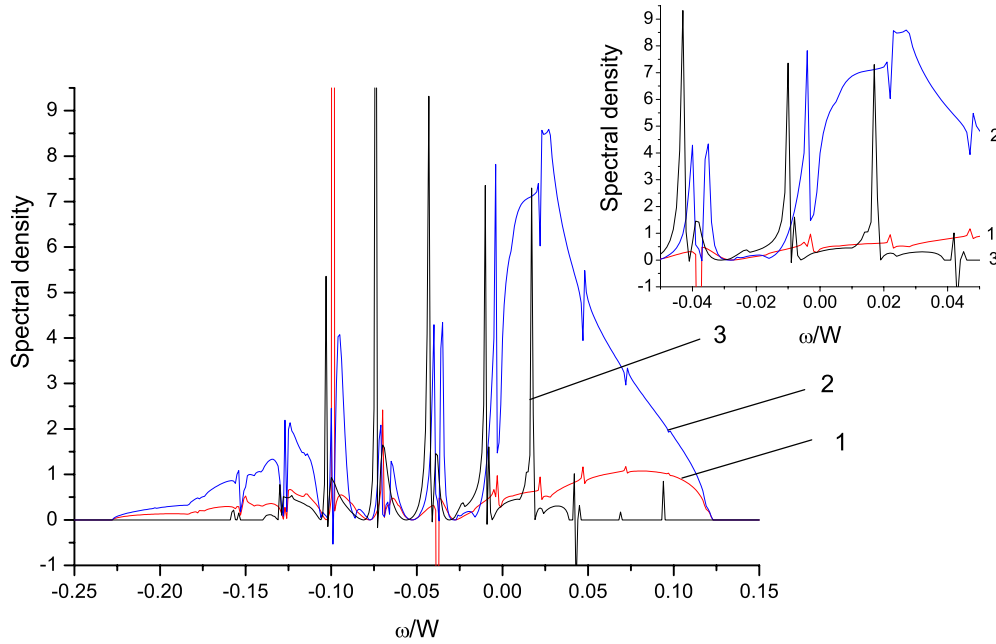


Figure 7. Spectral density versus frequency obtained using the approximation (equation (31)) for effective interaction at $\xi = 0.03$, $t(\mathbf{q})/W = 1/3$, $n = 0.8$ and $T/W = 0.005$ for up- and down-spin bands (curves 1 and 2, respectively) and for the PM phase at $T/W = 0.0123$ (curve 3). Inset: the same plot near zero frequency on an enlarged scale. The chemical potentials in the FM and PM phases are equal to 0.0277 and 0.0311, respectively (in units of W).

(This figure is in colour only in the electronic version)

The expression for the conductivity $\sigma(T)$ of the s.c. lattice obtained on the basis of the above results using the Kubo formula in the bubble approximation [5] has the form

$$\sigma(T) = \frac{e^2}{3a\pi\hbar N} \sum_{\mathbf{q}\sigma} \Phi_{\sigma}(t(\mathbf{q}))t(\mathbf{q}),$$

where the $\Phi_{\sigma}(t(\mathbf{q}))$ function is related to the spectral density by the following differential equation:

$$\frac{d\Phi_{\sigma}(t(\mathbf{q}))}{d(t(\mathbf{q}))} = [R_{\sigma}(\omega, \mathbf{q})]^2. \quad (47)$$

Since the imaginary part of the Green function (equation (46)) is a simple function of the parameter $t(\mathbf{q})$, the integration of the squared spectral density in equation (47) presents no problem. Here we are not presenting a sufficiently complicated expression for $\Phi_{\sigma}(t(\mathbf{q}))$.

In figure 8 the resistivity versus band filling ($\rho(n)$) in the FM and PM-2 phases (curves 1 and 2, respectively) are shown at $T = 0$ and $\xi = 0$. Curve 3 in figure 8 shows the dependence of $\rho(n)$ in the PM phase calculated by the CPA method [5, 21]. It is seen from figure 8 that the CPA method gives a minimal $\rho(n)$ value of the order of 1 m Ω cm. In our case the resistivity $\rho(n)$ in the PM-2 and FM phases is much smaller near their lower boundaries at $n \geq n_0$ (n_0 is equal to 0.116 and 0.588 for the PM-2 and FM phases, respectively). According to the experimental data [22] in $\text{La}_{1-x}\text{Sr}_x\text{MnO}_3$ the residual resistance at $x \sim 0.3$ is essentially smaller than 1 m Ω cm. At $n \rightarrow 1$ the resistivity $\rho(n)$ in the FM phase abruptly increases, as in the CPA method.

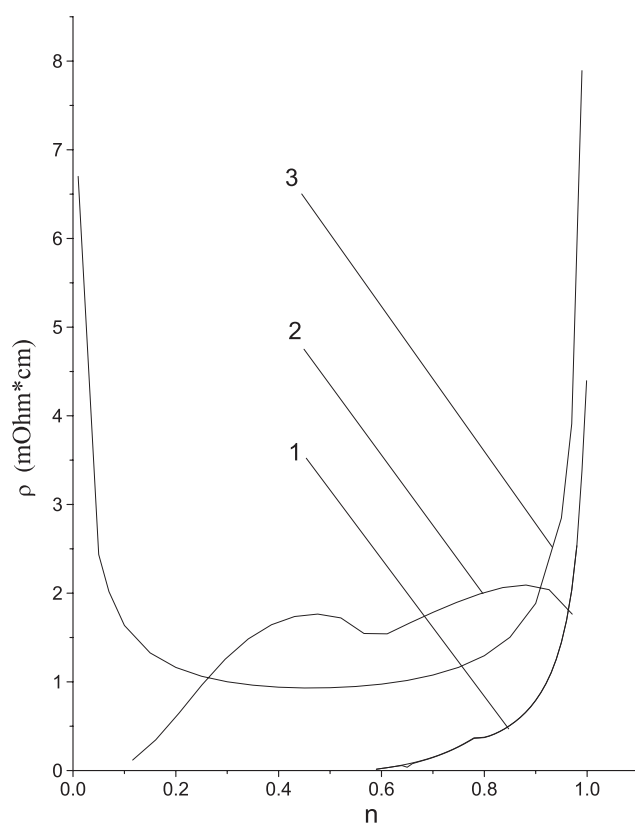


Figure 8. Resistivity $\rho(n)$ in the DE model for the FM and PM-2 phases (curves 1 and 2, respectively) at $T = 0$, $h = 0$. Curve 3 is obtained using the coherent potential approximation (CPA) [5].

Figure 9(a) gives the temperature dependence of resistivity at $n = 0.8$ neglecting electron–phonon coupling. In the inset of figure 9(a) a comparison of calculated $\rho(T)$ at $W = 1$ eV [10], $n = 0.8$ and 0.6 with the experimental temperature dependence of the resistivity for $\text{La}_{0.7}\text{Sr}_{0.3}\text{MnO}_3$ film [23] is shown. One can see the qualitative agreement between theory and experiment. We have also calculated the curve $\rho(T)$ at $n = 0.6$, since the value of residual resistivity ρ_0 in this case agrees well with that of experiment [23] for $\text{La}_{0.7}\text{Sr}_{0.3}\text{MnO}_3$ film. Unlike the CPA method, a sufficiently abrupt growth of resistivity near the phase transition with increasing T is seen. Figure 9(b) gives the temperature dependences of the imaginary parts $\Lambda_4^\sigma(\omega)$ and $\Delta_6^\sigma(\omega)$ at $\omega = 0$. A sharp increase of some dependences in value near T_C reflects the essential strengthening of scattering processes near the phase transition. In the PM-2 phase the resistivity is weakly dependent on temperature, and its maximal value does not exceed several $\text{m}\Omega \text{ cm}$, as observed in [5]. The authors of [6, 11, 21] pointed out that this is a characteristic property of systems with dominant DE such as $\text{La}_{1-x}\text{Sr}_x\text{MnO}_3$. In $\text{La}_{1-x}\text{Ca}_x\text{MnO}_3$ compounds the polaron dynamics becomes important because of stronger electron–phonon coupling.

In figure 10 the influence of weak electron–phonon interaction on the $\rho(T)$ -dependence calculated using the approximation (31) for the effective line at $n = 0.8$ is shown. Indeed, a large number of polarons participate in the conductivity and increase it above T_C . It is seen that

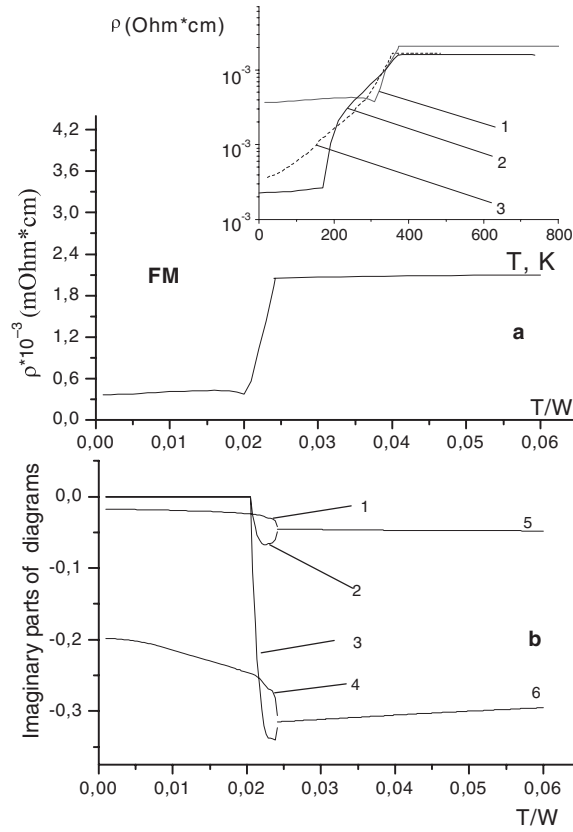


Figure 9. In the DE model the $\rho(T)$ dependences (a) and imaginary parts of $\Delta_6^\sigma(\omega)$ and $\Lambda_4^\sigma(\omega)$ (b) diagrams at $n = 0.8$ and $\omega = 0$ (curves 1, 3 and 2, 4 for up- and down-spin band, respectively). Curves 5 and 6 are the same plots for $\Delta_6^\sigma(\omega)$ and $\Lambda_4^\sigma(\omega)$ in the PM-2 phase, respectively. In the inset a comparison of experimental (curve 3) for $\text{La}_{1-x}\text{Sr}_x\text{MnO}_3$ with $x = 0.3$ [23] and theoretical at $W = 1$ eV, $n = 0.8$ (curve 1) and $n = 0.6$ (curve 2) resistivities is shown.

the resistivity changes from a ‘metallic’ ($d\rho/dT > 0$) to an ‘insulating’ ($d\rho/dT < 0$) regime with increasing polaron binding energy in the PM phase. This agrees with the previous results obtained in [6, 11, 21]. However, the resistivity falls off with increasing polaron binding energy ξ . The discrepancy between calculated and experimental values of the maximum resistivity is due to the influence of vertex corrections in current correlators which are ignored in the bubble approximation. Another reason is that we use the approximation (31) for the effective line in the limit of strong electron–phonon coupling.

7. Conclusions

We have considered the magnetic, transport and spectral properties of manganites in the framework of the Holstein DE model. In the case of a narrow-band Hubbard magnet the unitary transformation is found to build the diagram techniques with the allowance for strong Hund’s rule coupling ($J_H \gg W$). It may be stated that the quantum fluctuations of electron and ion spins play an important role in the magnetic ordering of manganites. In particular, it is the fluctuations of spin $S = 2$ that reduce the Curie temperature by approximately 30%.

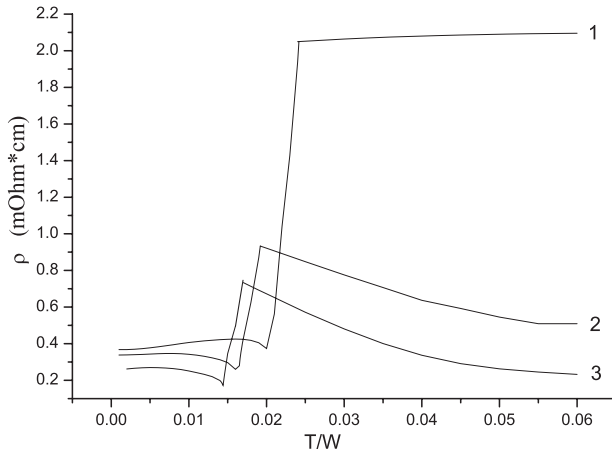


Figure 10. Influence of weak electron-phonon interaction on $\rho(T)$ at $n = 0.8$ and $h = 0$ for polaron binding energy ξ/W : 0, 0.003 and 0.005 (curves 1–3, respectively).

Results are given for the effects of electron-phonon interactions. Unfortunately, the equation obtained for pole singularities of the Green function is very complex. Using the approximation having regard to a few polaron bands, the strong influence of electron-phonon interaction on T_C as well as on magnetization was established. This agrees with theoretical predictions of both dynamic mean-field and coherent potential approximations.

The analysis of the temperature dependence of resistivity in the framework of the considered model shows that the $\rho(T)$ -dependence rises rapidly at the phase transition from FM to PM state (as in $\text{La}_{1-x}\text{Sr}_x\text{MnO}_3$ with optimal Sr content). The spectral density as a function of T reflects the enforcing of scattering effects near the Curie temperature. For the pure DE model the minimal residual resistance was shown to be smaller than that obtained in the CPA theory. This result agrees with that of experiments for some perovskite manganites and confirms the correct treatment of the electron scattering.

In the double-exchange model the analysis of spectral density shows the shift of maximum $R_{\uparrow}(\omega, \mathbf{k})$ to Fermi energy for wavevectors to be changed from the edge to the centre of the Brillouin zone. Qualitative agreement was obtained between calculated and experimental APRES spectra. In the PM phase the temperature dependence of resistivity changes from a ‘metallic’ ($d\rho/dT > 0$) to an ‘insulating’ ($d\rho/dT < 0$) regime with increasing polaron binding energy. The increase of conductivity above T_c with increasing temperature can be caused by the presence of pronounced polaron peaks in the spectral density. However, the decrease in the peak height of resistivity with increasing polaron binding energy indicates that additional work is needed to improve the accuracy of the approximation used for effective electron-phonon interaction.

Acknowledgment

This work was in part supported by the Polish Government Agency KBN (Project 1 P03B 025 26).

Appendix

The annihilation operators are expressed as

$$\begin{aligned} c_{\uparrow} &= L^{9,1} + \frac{\sqrt{3}}{2}L^{10,2} + \frac{1}{\sqrt{2}}L^{11,3} + \frac{1}{2}L^{12,4} \\ c_{\downarrow} &= \frac{1}{2}L^{9,2} + \frac{1}{\sqrt{2}}L^{10,3} + \frac{\sqrt{3}}{2}L^{11,4} + L^{12,5}. \end{aligned} \quad (\text{A.1})$$

To obtain similar formulae for the electron creation operators the Hermitian conjugate of (A.1) was performed. Since we used the wavefunctions of model space in which the $|\varphi_6\rangle$, $|\varphi_7\rangle$ and $|\varphi_8\rangle$ functions of orthogonal add-ins are excluded, the equality $c^\dagger c + c c^\dagger = 1$ fails for Fermi operators. However, this is not important under this consideration because Wick's theorem is used directly on Hubbard operators for which the Fermi or Bose origin does not break down.

The operators of electron n and hole p numbers have the form

$$\begin{aligned}\hat{n} &= L^{1,1} + L^{2,2} + L^{3,3} + L^{4,4} + L^{5,5} \\ \hat{p} &= L^{9,9} + L^{10,10} + L^{11,11} + L^{12,12}.\end{aligned}\quad (\text{A.2})$$

In this case $p + n = 1$. The operators of electron n_σ and hole p_σ numbers with spin σ are determined as follows:

$$\begin{aligned}\hat{n}_\uparrow &= L^{1,1} + \frac{3}{4}L^{2,2} + \frac{1}{2}L^{3,3} + \frac{1}{4}L^{4,4} \\ \hat{n}_\downarrow &= \frac{1}{4}L^{2,2} + \frac{1}{2}L^{3,3} + \frac{3}{4}L^{4,4} + L^{5,5} \\ \hat{p}_\uparrow &= L^{9,9} + \frac{3}{4}L^{10,10} + \frac{1}{2}L^{11,11} + \frac{1}{4}L^{12,12} \\ \hat{p}_\downarrow &= \frac{1}{4}L^{9,9} + \frac{1}{2}L^{10,10} + \frac{3}{4}L^{11,11} + L^{12,12}\end{aligned}\quad (\text{A.3})$$

and the following relations

$$\begin{aligned}\hat{n}_\uparrow + \hat{n}_\downarrow &= \hat{n}, & \hat{p}_\uparrow + \hat{p}_\downarrow &= \frac{5}{4}(1 - \hat{n}) \\ \hat{n}_\uparrow - \hat{n}_\downarrow &= 2\sigma^z \\ \hat{p}_\uparrow - \hat{p}_\downarrow &= \frac{1}{2}S_0^z\end{aligned}\quad (\text{A.4})$$

take place. The z -projection of the spin operator S^z on the truncated basis of t_{2g} and e_g electrons is expressed as

$$S^z = \frac{3}{2}(L^{1,1} - L^{5,5} + L^{9,9} - L^{12,12}) + \frac{3}{4}(L^{2,2} - L^{4,4}) + \frac{1}{2}(L^{10,10} - L^{11,11}).$$

The imaginary parts of the $\Lambda_4^\sigma(\omega)$ and $\Delta_6^\sigma(\omega)$ functions after analytic continuation to the real axis $i\omega_n \rightarrow \omega + i\delta$ are written in the form (see approximation (31) with formulae (42) for $\Lambda_4^\sigma(\omega)$ and $\Delta_6^\sigma(\omega)$):

$$\begin{aligned}\text{Im}(\Lambda_4^\sigma(\omega)) &= -\frac{3\pi\sigma b(\varepsilon_{-\sigma\sigma})\langle\sigma^z + \frac{1}{4}S^z\rangle_0}{W\langle F^{-\sigma 0}\rangle^2} \\ &\times \sum_{m=-\infty}^{\infty} \Omega_{m\sigma}(\omega) \frac{P_0\varphi_{00}}{P_{-\sigma}\varphi_{m-\sigma}} D_C\left(\frac{6\Omega_{m\sigma}(\omega)}{\langle F^{-\sigma 0}\rangle P_{-\sigma}\varphi_{m-\sigma} W}\right)\end{aligned}\quad (\text{A.5})$$

$$\frac{1}{\beta} \text{Im}(\Delta_6^\sigma(\omega)) = -\frac{6\pi m(\tilde{\mu})}{W\langle F^{\sigma 0}\rangle^2} \sum_{m=-\infty}^{\infty} \left(\frac{\Omega_{m-\sigma}(\omega)}{P_\sigma\varphi_{m\sigma}}\right)^2 D_C\left(\frac{6\Omega_{m-\sigma}(\omega)}{\langle F^{-\sigma 0}\rangle P_\sigma\varphi_{m\sigma}}\right),\quad (\text{A.6})$$

where $\Omega_{m\sigma}(\omega) = \omega + \varepsilon_{0-\sigma} + m\omega_0$.

References

- [1] Anderson P W and Hasegawa H 1955 *Phys. Rev.* **100** 675
- [2] de Gennes P G 1960 *Phys. Rev.* **118** 141
- [3] Kubo K and Ohata N 1972 *J. Phys. Soc. Japan* **33** 21
- [4] Furukawa N 1994 *J. Phys. Soc. Japan* **63** 3214
- [5] Edwards D M, Green A C M and Kubo K 1999 *J. Phys.: Condens. Matter* **11** 2791
- [6] Green A C M 2001 *Phys. Rev. B* **63** 205110
- [7] Zubov E E 1993 *Low Temp. Phys.* **19** 193
- [8] Zubov E E 1995 *Theor. Math. Phys.* **105** 311
- [9] Zubov E E, Dyakonov V P and Szymczak H 2002 *J. Exp. Theor. Phys.* **95** 1044

- [10] Coey J M D and Viret M 1999 *Adv. Phys.* **48** 167
- [11] Millis A J, Mueller R and Shraiman B J 1996 *Phys. Rev. B* **54** 5405
- [12] Lang I G and Firsov Yu A 1963 *Sov. Phys.—JETP* **16** 1301
- [13] Biedenharn L C and Louck J D 1981 *Angular Momentum in Quantum Physics* (Reading, MA: Addison-Wesley)
- [14] Yang D H Y and Wang Y L 1974 *Phys. Rev. B* **10** 4714
- [15] Izyumov Yu A and Scryabin Yu N 1987 *Statistical Mechanics of Magnetically Ordered Systems* (Moscow: Nauka)
- [16] Mahan G D 1990 *Many-Particle Physics* (New York: Plenum)
- [17] Holstein T 1959 *Ann. Phys.* **8** 343
- [18] Jonker G H and Van Santen J H 1950 *Physica* **16** 337
Jonker G H and Van Santen J H 1953 *Physica* **19** 120
- [19] Larkin A I 1959 *Sov. Phys.—JETP* **37** 264
- [20] Dessau D S, Saitoh T, Park C H, Shen Z X, Villeda P, Hamada N, Moritomo Y and Tokura Y 1998 *Phys. Rev. Lett.* **81** 192
- [21] Edwards D M 2002 *Adv. Phys.* **51** 1259
- [22] Urushibara A, Moritomo Y, Arima T, Asamitsu A, Kido G and Tokura Y 1995 *Phys. Rev. B* **51** 14103
- [23] Coey J M D, Viret M, Ranno L and Ounadjela K 1995 *Phys. Rev. Lett.* **75** 3910